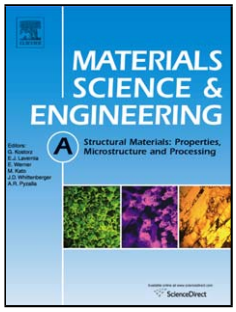

Title: In-Situ Diffraction Study on Decomposition of Ti_2AlN at 1500-1800 °C in Vacuum

Authors: W.K. Pang, I.M. Low, S.J. Kennedy, R.I. Smith

PII: S0921-5093(10)00871-3
DOI: doi:10.1016/j.msea.2010.08.012
Reference: MSA 26455

To appear in: *Materials Science and Engineering A*

Received date: 14-4-2010
Revised date: 31-7-2010
Accepted date: 4-8-2010

Please cite this article as: W.K. Pang, I.M. Low, S.J. Kennedy, R.I. Smith, In-Situ Diffraction Study on Decomposition of Ti_2AlN at 1500-1800 °C in Vacuum, *Materials Science & Engineering A* (2010), doi:10.1016/j.msea.2010.08.012

In-Situ Diffraction Study on Decomposition of Ti_2AlN at 1500-1800 °C in Vacuum

W.K. Pang[1], I.M. Low[1*], S.J. Kennedy[2], R.I. Smith[3]

[1]*Centre for Materials Research, Department of Imaging and Applied Physics, Curtin University of Technology, GPO Box U 1987, Perth WA, Australia*

[2]*The Bragg Institute, ANSTO, Locked Bag 2001, Kirrawee DC, NSW 2232, Australia*

[3]*ISIS Facility, Science and Technology Facilities Council, Rutherford Appleton Laboratory, Harwell Science and Innovation Campus, Didcot, Oxfordshire OX11 0QX, UK*

For: Materials Science & Engineering A

---

* Corresponding author. Tel.: +61-8-9266 7544; fax: +61-8-9266 2377

Email: j.low@curtin.edu.au

Abstract

The susceptibility of Ti_2AlN to thermal dissociation at 1500-1800 °C in high vacuum has been studied using *in-situ* neutron diffraction. Above 1500 °C, Ti_2AlN decomposed to TiN_x primarily through the sublimation of aluminium (Al). The kinetics of isothermal phase decomposition at 1550 °C was modelled using a modified Avrami equation. An Avrami exponent (*n*) of 0.338 was determined, indicative of the highly restricted **out**-diffusion of Al between the channels of Ti_6N octohedra. The characteristics of thermal stability and phase transition in Ti_2AlN are discussed. Characterisation of surface compositions and examination of cross-sectional microstructures of decomposed Ti_2AlN, using synchrotron radiation diffraction and SEM respectively, verify the findings of the neutron diffraction; that Ti_2AlN decomposes to TiN_x at the surface primarily via **the** sublimation of Al from grain boundaries.

1. Introduction

MAX phases are nano-layered ceramics with the general formula $M_{n+1}AX_n$ (n= 1-3), where M is an early transition metal, A is a group-A element, and X is either carbon or nitrogen. These materials exhibit mixed metallic and ceramic properties, e.g., low density, low thermal expansion coefficient, high modulus and high strength, and good high-temperature oxidation resistance of ceramics; and good electrical and thermal conductors, readily machinable, tolerant to physical damage, and resistant to thermal shock of metals [1-3]. *MAX* phases are **becoming technologically important because they display a** unique combination of **metallic and ceramic** properties, and **are thus potential** candidate materials for high temperature applications. Advances in the understanding of the high-temperature characteristics will enable the unique multi-functional properties of *MAX* phases to be fully utilised at elevated temperature.

However, there is a dearth of research regarding the thermal stability of these novel *MAX* phases, especially for ternary nitrides. This lack of information has caused much controversy on the high-temperature thermochemcial stability of *MAX* phases where conflicting results on the decomposition temperature have been reported [4-6]. In our previous investigations of the thermal stability of 312 phases (Ti_3SiC_2 and Ti_3AlC_2) and 211 phases (Ti_2AlC and Cr_2AlC) in vacuum at up to 1550 °C using *in-situ* constant-wavelength (CW) neutron diffraction, we found 211 phases to be more stable than 312 phases [7-12]. For instance, more than 45 wt% Ti_3AlC_2 decomposed into TiC at 1550 °C when compared to only 7 wt% for Ti_2AlC [10]. In addition, a positive activation energy of 85.7 $kJ.mol^{-1}$ was observed for Ti_2AlC whereas a negative activation energy of -71.9 $kJ.mol^{-1}$ was determined for Ti_3AlC_2 [9, 12].

The thermal stability of Ti_3SiC_2 thin films was investigated by Emmerlich *et al.* [13] and they attributed the rapid decomposition of thin films at 1100-1200 °C to the out-diffusion

of Si with the concomitant formation of oriented TiC_x (x=0.67). Radhakrishnan *et al.* [14] reported similar results for the decomposition of bulk Ti_3SiC_2 in vacuum and claimed that Ti_3SiC_2 did not decompose up to 1800 °C but was susceptible to carburization and oxidation. Oo *et al*. [15] reported that Ti_3SiC_2 decomposed into TiC and $Ti_5Si_3C_x$ at 1200 °C in argon **atmosphere** with low oxygen partial pressure. Moreover, the occurrence of transformation between α- and β- Ti_3SiC_2 was also reported by Sun *et al*. [16]

However, the fundamental knowledge about the thermal stability of technologically important *MAX* phases is still very limited and the actual process of phase dissociation is poorly understood. Hitherto, virtually no work has been reported for ternary nitrides such as Ti_2AlN and Ti_4AlN_3. It also remains unknown whether ternary nitrides will undergo the same decomposition process as ternary carbides via the evaporation of the high vapour pressure group A and M elements, i.e., [8, 9]

$$M_{n+1}AX_n \rightarrow nMX + A + M \qquad (1)$$

In this paper, we describe a time-of-flight (ToF) neutron diffraction study of the dynamics of phase stability of Ti_2AlN in high-vacuum at elevated temperatures (1500 ºC to 1800 ºC). The use of neutron diffraction allows the bulk information on decomposition of Ti_2AlN to be obtained by virtue of the bulk sampling and penetrating nature of neutrons. In addition, it allows the dynamic measurements under non-ambient conditions to be conducted with ease. The kinetics of isothermal phase decomposition was modelled using the Avrami equation and the Avrami constants were evaluated. The characteristics of thermal stability and phase transitions in Ti_2AlN have been evaluated and discussed.

2. Experimental Procedure

2.1 Material synthesis

Dense hot-pressed cylindrical Ti_2AlN samples of 10 mm diameter and 20 mm height were used in this study. The samples contained 6.9 wt% TiN and had ≤0.5% porosity. The samples were prepared by hot-pressing of powder mixture of TiN (99.3% purity, 2.03 μm), Ti (99.0% purity, 2.48 μm) and Al (99.8% purity, 1.50 μm). The powders were mixed in the molar ratio of 1Ti : 1Al :1TiN. The mixture was initially mixed in ethanol for 24 h, and then hot-pressed in Ar atmosphere at a rate of 50 ºC/min until the temperature of 1400 ºC was reached, and dwelled for 2 h. The pressure used during hot-pressing was 30MPa.

2.2 In-situ high temperature neutron diffraction

The *in-situ* ToF neutron diffraction was used to monitor the structural evolution of phase decomposition in Ti_2AlN at high temperature in real time. Diffraction patterns were collected using the Polaris medium resolution, high intensity powder diffractometer at the UK pulsed spallation neutron source ISIS, Rutherford Appleton Laboratory.

Samples were held in a basket made from thin tantalum wire and mounted in a Risø-design high temperature furnace (Risø National Laboratory, Roskilde). Fitted with a thin tantalum foil element and tantalum and vanadium heat shields, this furnace is capable of reaching 2000°C and operates under a high dynamic (i.e. continuously pumped) vacuum (pressure < 7.5×10^{-6} torr). Temperature monitoring and control was achieved using type W5 thermocouples connected to Eurotherm 3504 controllers. Collimating slits (manufactured from neutron-absorbing boron nitride) mounted on the furnace in the scattered beam direction enable diffraction patterns free from Bragg reflections off the tantalum element and heat shields to be collected in the Polaris $2\theta = 90°$ detectors. A precision electronic scale (reading to five decimal places) was used to weigh the sample before it was loaded into the furnace.

For each sample, a reference diffraction pattern was collected at room temperature while the furnace was initially evacuated, then the sample was heated rapidly up to a selected

temperature (e.g. 1500, 1550, 1600, 1700, and 1800 °C) where it was held constant for an extended period during which a series of diffraction patterns, each of 15 minutes duration, were collected. The total time spent at each elevated temperature was manually controlled, based on the level of decomposition observed in the diffraction patterns as they were collected.

At the end of each high temperature measurement the furnace was cooled to room temperature, and the sample carefully removed from the furnace and weighed again in order to determine the mass of titanium and aluminum lost through evaporation.

Normalised data collected in the Polaris 90° detector bank over the *d*-spacing range of ~0.4-3.2Å were analysed using Rietveld software - Fullprof [17] to compute the changes in Ti_2AlN and TiN contents during vacuum annealing. The Rietveld strategy of the refinement process for the neutron diffraction data is summarised in Table 1.

The kinetics of isothermal decomposition of Ti_2AlN at 1550 °C was modelled using the Avrami equation to describe the fraction of decomposed Ti_2AlN (y) as a function of time [18]:

$$y = \exp(-kt^n) \qquad (2)$$

where k and n are Avrami rate constant and Avrami exponent for the particular reaction. The rate constant k relates to the rate of reaction which in **this** study refers to the decomposition rate of Ti_2AlN in vacuum. In general, when the value of n is large (e.g. 3 or 4), a 3-dimensional nucleation and growth processes are involved. High values of n can occur when nucleation occurs on specific sites such as grain boundaries or impurities which rapidly saturate soon after the transformation begins.

2.3 Synchrotron radiation diffraction (SRD)

The SRD data were collected using beam-line BL-20B at the Photon Factory in Japan. A diamond blade was used to cut thin slices (~1 mm thick) from the as-annealed samples

following the high-temperature neutron diffraction experiment described above. The cut slices were then ultra-sonically cleaned prior to SRD experiments. The diffraction patterns of thermally decomposed Ti_2AlN samples were recorded at an incident angle of 3.0° with a fixed wavelength of 0.7 Å. The computer program "*DIFFRA*^{plus} EVA" was used to identify the crystalline phases present.

2.4 Scanning electron microscopy

The cross-sectional microstructures of vacuum-decomposed Ti_2AlN following the neutron diffraction experiment were examined using Zeiss (Oberkochen, Germany) EVO 40XVP SEM with an accelerating voltage of 15 keV. The sample was not gold or carbon-coated before the microstructure examination by virtue of its high electrical conductivity and the images were taken using secondary electrons.

3. Results and Discussion

3.1 Phase evolution during Ti_2AlN decomposition

The Rietveld method was used to analyze the neutron diffraction patterns. The goodness-of-fit (χ^2) ranged from 1.4 to 3.9. Typical plots of Rietveld profile fit are shown in Fig. 1(a) and Fig. 1(b) for Ti_2AlN before and after vacuum decomposition at 1550°C. The phase transformations of Ti_2AlN at various temperatures as revealed by *in-situ* TOF neutron diffraction are shown in Figure 2a. An increase in TiN_x content due to decomposition of Ti_2AlN was observed with an increase in temperature from 1400 to 1800°C. Ti_2AlN began to decompose into TiN_x slowly at 1550 °C (i.e. < 10% in the first hour) but became quite rapid at 1600 °C (i.e. ~ 90 % in the first hour). The sample was almost completely decomposed after annealing at 1700 °C for 2 hours and at 1800 °C for about 20 min. The weight loss was 5.0% and 0.95% at 1550 and 1500 °C, respectively, whereas nearly 20% weight loss was

observed for decomposition at 1600 °C and above. Noting that there is about 19.7 wt% of Al in Ti_2AlN, we deduce that the weight loss in decomposed Ti_2AlN is entirely due to **the** sublimation of Al when its vapour pressure rises above the ambient pressure of the furnace. This is not surprising when we consider that the vapour pressure of Al metal rises rapidly from ~7 x 10^{-3} torr at 1200 °C to ~0.5 torr at 1500 °C [19]. By contrast the vapour pressure for Ti metal is more than three orders of magnitude lower in this temperature range [19]. Thus, at temperatures higher than 1500 °C, we might expect Al to become quite volatile and sublime continuously in a dynamic environment of high vacuum, leading to severe decomposition of Ti_2AlN with the concomitant formation of non-stoichiometric TiN_x, i.e.,

$$Ti_2AlN_{(s)} \xrightarrow{T \geq 1500^{o}C} 2TiN_{0.5(s)} + Al_{(g)} \qquad (3)$$

This conclusion was strongly supported by visual inspection of samples and furnace inserts after decomposition, where aluminium coatings covered most surfaces. The formation of a TiN_x surface layer is further verified by the synchrotron radiation diffraction results of vacuum-decomposed Ti_2AlN at 1550 °C shown in Fig. 3.

Fig. 2(b) shows a comparison in diffraction patterns at 1550 and 1600 °C and highlights the formation of Ti_4AlN_3 at 1600 °C. Interestingly, formation of some Ti_4AlN_3 was also observed during the isothermal annealing of Ti_2AlN at 1600 °C as indicated in Fig. 4(a). A comparison between the diffraction patterns after soaking times of 10 and 90 minutes at 1600 °C is shown in Fig. 4(b). This process of 211 → 413 transformations has also been reported by Hu *et al.* [20-21] for the decomposition of Ta_2AlC into Ta_4AlC_3 and Nb_2AlC to Nb_4AlC_3 in argon **atmosphere** at high temperature, probably *via* the intercalation of the formed binary carbide (e.g. TaC) into the 211 structure (e.g. Ta_2AlC).

We propose that the formation of Ti_4AlN_3 during vacuum annealing of Ti_2AlN at 1600 °C occurs *via* the intercalation of TiN in Ti_2AlN as follows:

$$Ti_2AlN_{(s)} + 2TiN_{(s)} \xrightarrow{1600^{o}C} Ti_4AlN_{3(s)} \quad (4)$$

The processes of Ti_2AlN decomposition and the subsequent intercalation with TiN to form Ti_4AlN_3 are shown schematically in Fig. 5(a - d). A layered structure of Ti_2AlN is shown in Fig. 5(a) which gradually releases its Al elements from the structure when the temperature reaches about 1500 °C. Eventually, the edge-sharing tetrahedral formed non-stoichiometric TiN_x. At higher temperature (i.e. 1600 °C), TiN_x intercalated into Ti_2AlN layered structure as an extra layer of edge-sharing tetrahedral, leading to the formation of Ti_4AlN_3 as shown in Fig. 5(d). However, at temperatures above 1600 °C, Ti_4AlN_3 becomes unstable and decomposes into TiN_x *via* the sublimation of Al:

$$Ti_4AlN_{3(s)} \xrightarrow{T \geq 1600^{o}C} 4TiN_{0.75(s)} + Al_{(g)} \quad (5)$$

3.2 Avrami kinetics of isothermal phase decomposition

The isothermal phase evolution of Ti_2AlN during vacuum-annealing at 1550 °C was fitted with the modified Avrami equation (see Figs. 6a & 6b) The Avrami rate constant (k) and Avrami exponent (n) were determined to be 3.15×10^{-2} min^{-n} and 0.338, respectively. Since the obtained value of n is less than 1.0, this implies that the decomposition process is driven by the highly restricted outward diffusion of Al from the bulk to the surface of the sample and into the vacuum. In addition, when the vapour pressure of Al exceeds the ambient pressure in the vacuum furnace, bubbles will form inside the bulk of the substance which eventually appears as voids within the surface layer of decomposed Ti_2AlN, as shown in Figs. 7 & 8. The observed porous microstructure of TiN_x surface layer is analogous to the decomposition of Ti_3AlC_2 where fine pores also form on the TiC surface layer due to sublimation of Al elements from the bulk [9].

4. Conclusions

The high-temperature thermal stability of Ti_2AlN in a high vacuum has been studied using *in-situ* TOF neutron diffraction. Ti_2AlN was susceptible to decomposition above 1500 °C through sublimation of high vapour pressure Al elements, resulting in a porous surface layer of TiN_x ($0.5 \leq x \leq 0.75$) being formed. The kinetics of isothermal phase decomposition was modelled using the Avrami equation. The Avrami constants (k and n) of isothermal decomposition of Ti_2AlN were 3.15×10^{-2} min^{-n} and 0.338, respectively, the latter indicative of the highly restricted diffusion of Al between the channels of Ti_6N octahedron.

Acknowledgements

This work was funded by an ARC Discovery-Project grant (DP0664586) and an ARC Linkage-International grant (LX0774743). The collection of neutron diffraction data was conducted at ISIS (RB920121) which was provided by the Science and Technology Facilities Council, with financial support from an AMRFP grant. The collection of synchrotron diffraction data at the Photon Factory was funded by the Australian Synchrotron (AS101/ANBF2052).

References

[1] M.W. Barsoum, *Prog. Solid State Chem*. 28 (2000) 201.

[2] H.B. Zhang, Y.W. Bao and Y.C. Zhou, *J.Mater. Sci. Technol.* 25 (2009) 1.

[3] M.W. Barsoum and T. El-Raghy, *Am. Sci.* 89 (2001) 334.

[4] M.W. Barsoum and T. El-Raghy, *J. Am. Ceram. Soc*. 79 (1996) 1953.

[5] R. Radakrishnan, J.J. Williams and M. Akinc, *J. Alloys Compd*. 285 (1999) 85.

[6] J. Emmerlich, D. Music, P. Eklund, *et al*., *Acta Mater*. 55 (2007) 1479.

[7] I.M. Low and Z. Oo, *J. Aust. Ceram. Soc*. 38 (2002) 112.

[8] I.M. Low, *Mater. Lett.* 58 (2004) 927.

[9] W.K. Pang, I.M. Low and Z.M. Sun, *J Am. Ceram. Soc.* In press.

[10] W. K. Pang and I.M. Low, *J.Aust. Ceram. Soc.* 45 (2009) 39.

[11] W.K. Pang, I.M. Low, B.H. O'Connor, *et al.*, *J. Aust. Ceram.Soc.* 45 (2009) 72.

[12] W. K. Pang, I.M. Low, B.H. O'Connor, *et al.*, *J. Physics: Conf. Series*. In press.

[13] J. Emmerlich, D. Music, P. Eklund, *et al.*, *Acta Mater*. 55 (2007) 1479.

[14] R. Radhakrishnan, J. J. Williams and M. Akinc, *J. Alloys Compd*. 285 (1999) 85.

[15] Z. Oo, I. M. Low and B. H. O'Connor, *Physica B* 385-386 (2006) 499.

[16] Z. Sun, J. Zhou, D. Music, R. Ahuja and J. M. Schneider, *Scripta Mater*. 54 (2006) 105.

[17] http://www.ill.eu/sites/fullprof/

[18] J.W. Cahn, *Acta Metallurgica* 4 (1956) 572.

[19] www.veeco.com/library/Learning_Center/Growth_Information/Vapor_Pressure_ Data_For_ Selected_Elements /index.aspx

[20] C. Hu, J. Zhang, Y. Bao, J. Wang, M. Li, Y. Zhou, *Z. Metallkd*. 99 (2008) 8.

[21] C. Hu, F. Li, J. Zhang, J.M. Wang, J.Y. Wang, Y. Zhou, *Scripta Mater*. 57 (2007) 893.

Tables

Table 1. Refinement strategy of the Rietveld method for ToF neutron diffraction data.

Category	Setting/Value(s)
Software	WinPlotR/Fullprof
Refinement weighting model	Newton-Raphson algorithm least-square
Peak shape modelling	T.O.F. pseudo-Voigt * B-t-B exponential
ToF-*d*-spacing conversion	$\mathrm{ToF} = \mathrm{DIFC} \times \mathrm{d} + \mathrm{DIFA} \times \mathrm{d}^2 + ZERO$ DIFC= 4571.84 (fixed) DIFA= -0.69 (refinable) ZERO= 1.9 (fixed)
Refining region in ToF	1500 - 19200 μsec (~0.3 - 4.3Å)
Batch refinement strategy	Dual-direction sequential refinement (from starting point to ending point; and from ending point to starting point).
Assessing parameters	$\mathrm{R}_{\mathrm{wp}} = \left\{ \frac{\sum w_i [Y_i(obs) - Y_i(calc)]^2}{\sum w_i [Y_i(obs)]^2} \right\}^{\frac{1}{2}}$ $\mathrm{R}_{\mathrm{exp}} = \left[\frac{N-P}{\sum w_i Y_i^2(obs)} \right]^{1/2}$ $\chi^2 = GOF = \left[\frac{R_{wp}}{R_{\mathrm{exp}}} \right]^2 = \frac{\sum w_i [Y_i(obs) - Y_i(calc)]^2}{N-P}$ Noted that Y_i(obs) is the observed intensity and Y_i(calc) is the intensity calculated at point *i*, and w_i is the weighting factor or reciprocal of Y_i(obs) for point *i* in the whole pattern. *N* is the number of observations; *P* is the number of adjusted parameters; *N-P* is the weighed sum of squared residuals.

Figure Captions

1. The Rietveld profile fit of diffraction data of Ti_2AlN collected (a) before decomposition at 20°C {χ^2 = 1.4 ; R_{wp} = 33.8; R_{exp} = 28.4} and (b) after vacuum annealing at 1550°C {χ^2 = 3.9; R_{wp} = 38.0; R_{exp} = 19.0}. Measured patterns indicated by crosses, calculated pattern indicated by solid line. Intensity differences between the two patterns are shown along the bottom of the plot. Vertical bars represent the allowable peak positions for each of the phases. [Top: 211, Bottom: TiN]

2. (a) Phase transitions during the decomposition of Ti_2AlN from 1100°C to 1800°C in vacuum. Note the appearance of the Ti_4AlN_3 phase at 1600 ºC and *d*-spacing of ~ 3 Å. (b) A close-up view of the existence of Ti_4AlN_3 phase at 1600 ºC.

3. Synchrotron radiation diffraction pattern showing the formation of TiN_x at the near-surface of vacuum-decomposed Ti_2AlN at 1550 °C.

4. (a) Diffraction patterns of Ti_2AlN at room temperature (RT), 1100 and 1600°C with dwell times of 10, 30, 50, 70, and 90 minutes. Note that the formation of Ti_4AlN_3 at 1600°C; (b) A close-up view of the time-dependent growth of Ti_4AlN_3 phase at 1600 ºC.

5. Schematics showing the formation of Ti_4AlN_3 during the decomposition of Ti_2AlN *via* intercalation with TiN: (a) Ti_2AlN layered structure, (b) exclusion of Al *via* sublimation in vacuum, (c) formation of TiN from total depletion of Al in Ti_2AlN, and (d) intercalation of TiN into Ti_2AlN structure to form Ti_4AlN_3. (Legend: green bar = edge-sharing octahedral NTi_6, red circle = Al element)

6. (a) Phase abundance of Ti_2AlN at 1550 °C as a function of time and (b) phase reduction of Ti_2AlN showing the fitting with Avrami equation.

7. Scanning electron micrographs showing the surface microstructure of Ti_2AlN; (a) as-received and (b) after vacuum-annealing at 1550 °C.

8. Scanning electron micrograph showing the cross-sectional surface features of vacuum-decomposed Ti_2AlN at 1550 °C.

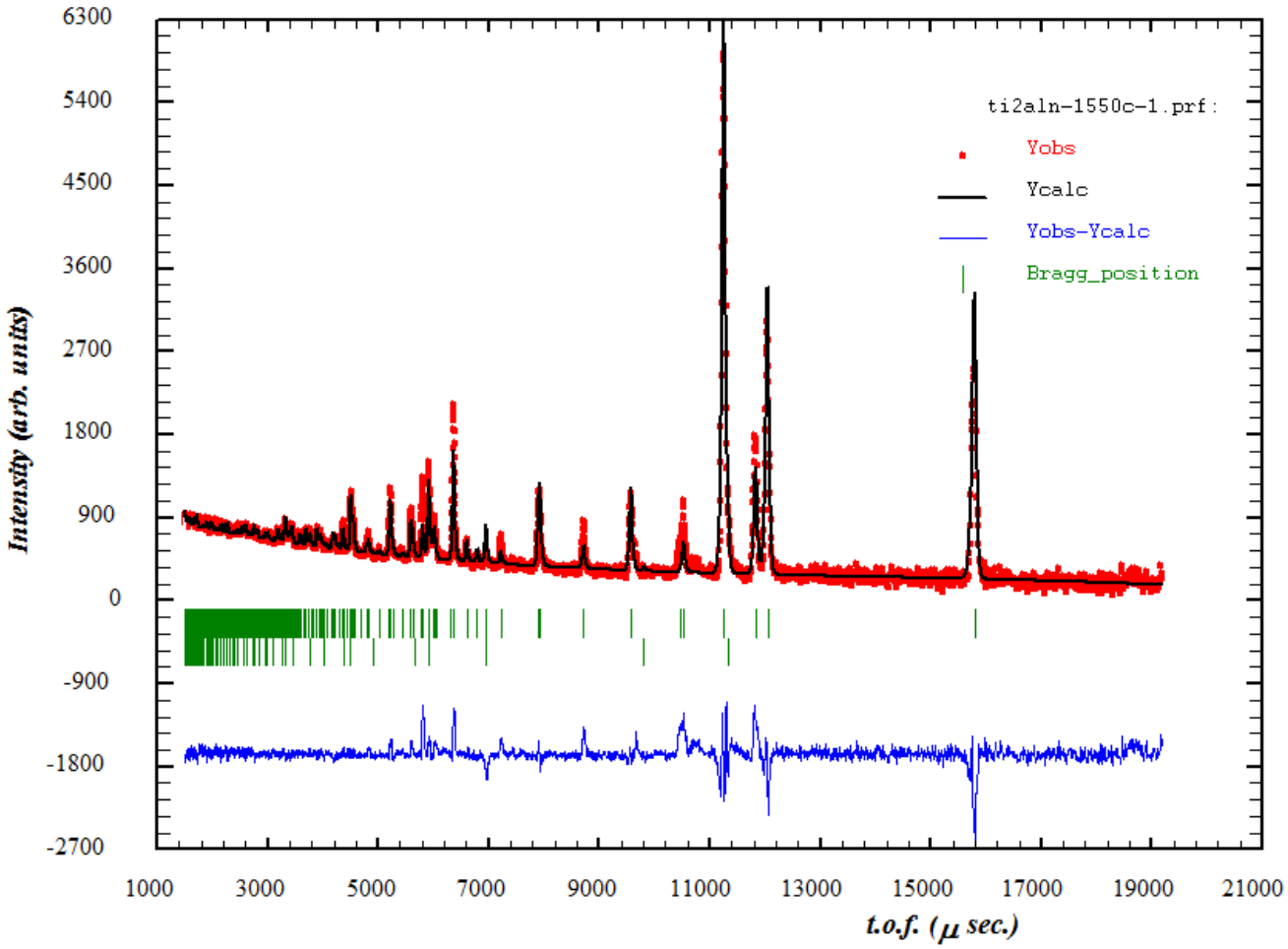

(a)

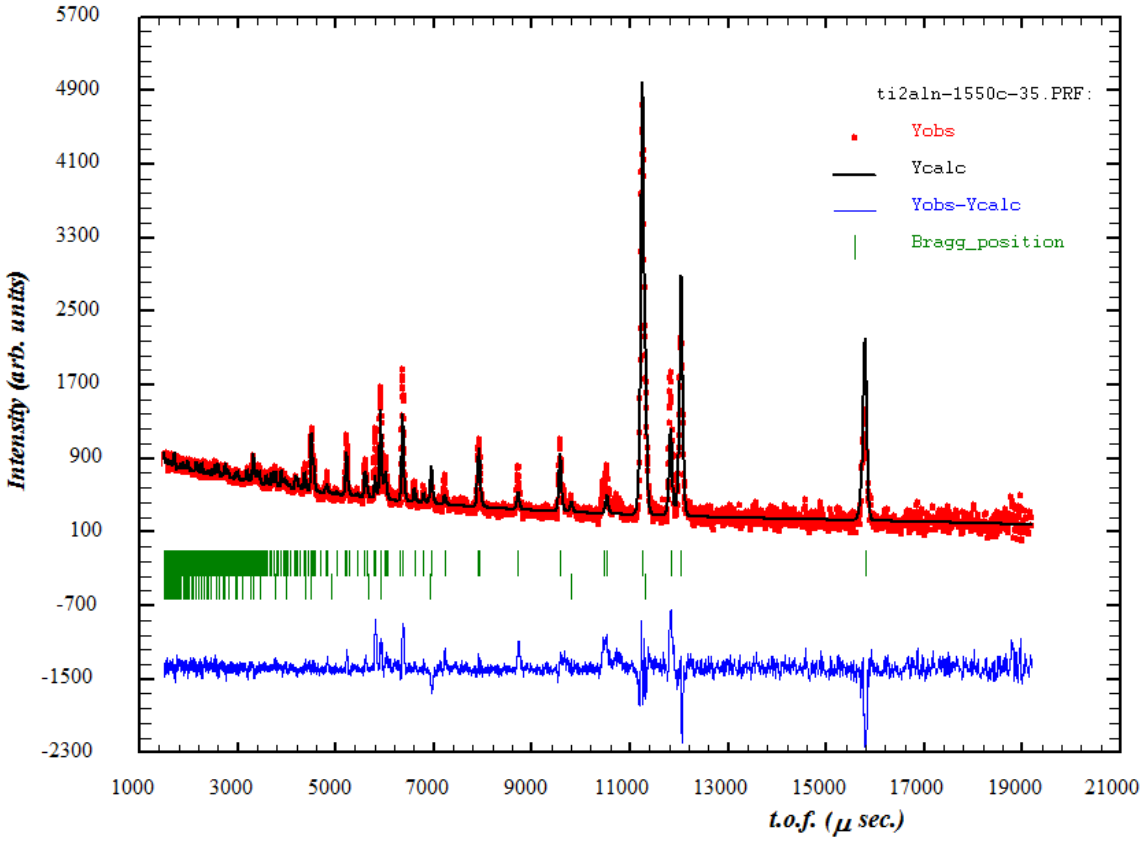

(b)

Figure 1: The Rietveld profile fit of diffraction data of Ti_2AlN collected (a) before decomposition at 20°C {χ^2 = 1.4 ; R_{wp} = 33.8; R_{exp} = 28.4} and (b) after vacuum annealing at 1550°C {χ^2 = 3.9; R_{wp} = 38.0; R_{exp} = 19.0}. Measured patterns indicated by crosses, calculated pattern indicated by solid line. Intensity differences between the two patterns are shown along the bottom of the plot. Vertical bars represent the allowable peak positions for each of the phases. [Top: 211, Bottom: TiN]

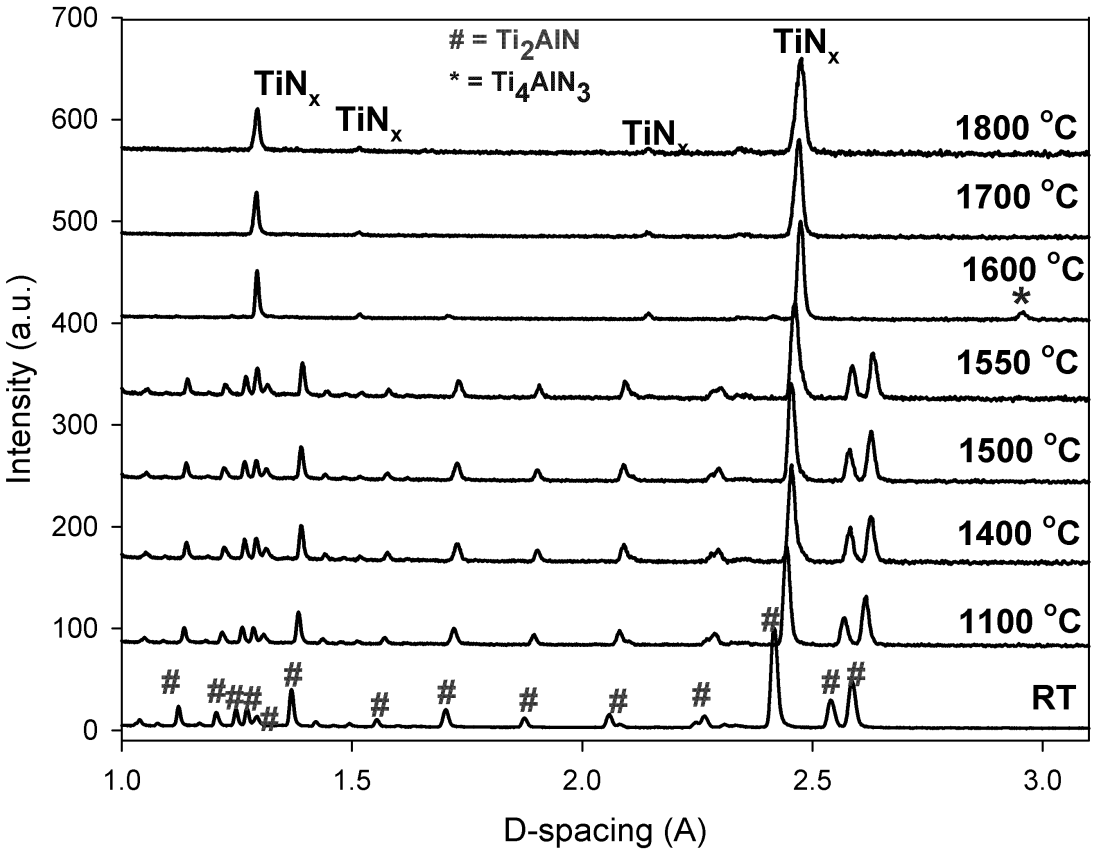

(a)

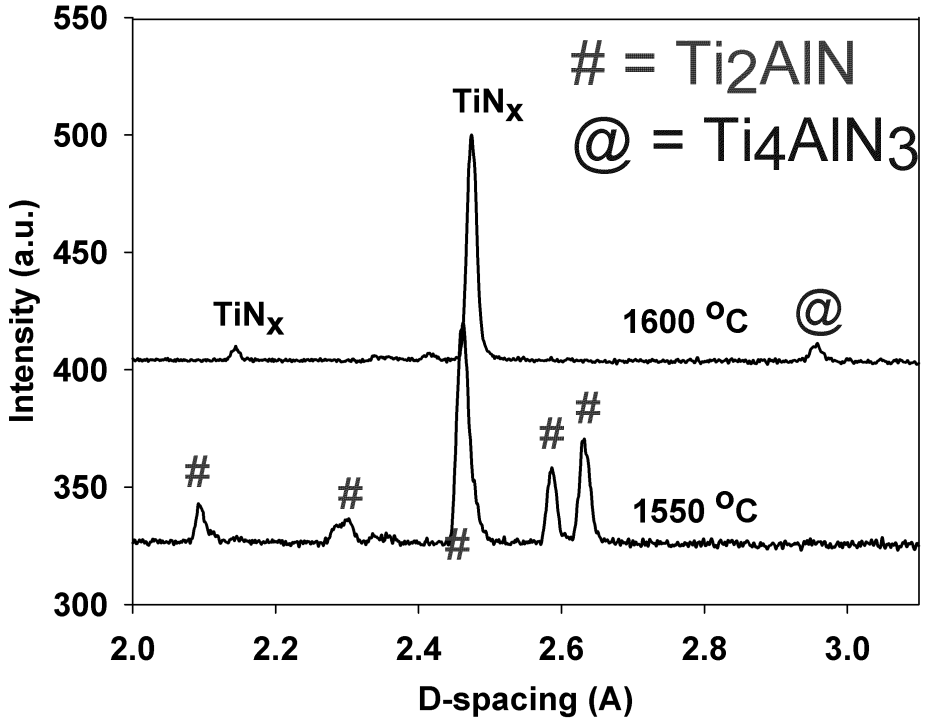

(b)

Figure 2: (a) Phase transitions during the decomposition of Ti_2AlN from 1100°C to 1800°C in vacuum. Note the appearance of the Ti_4AlN_3 phase at 1600 ºC and *d*-spacing of ~ 3 Å. (b) A close-up view of the existence of Ti_4AlN_3 phase at 1600 ºC.

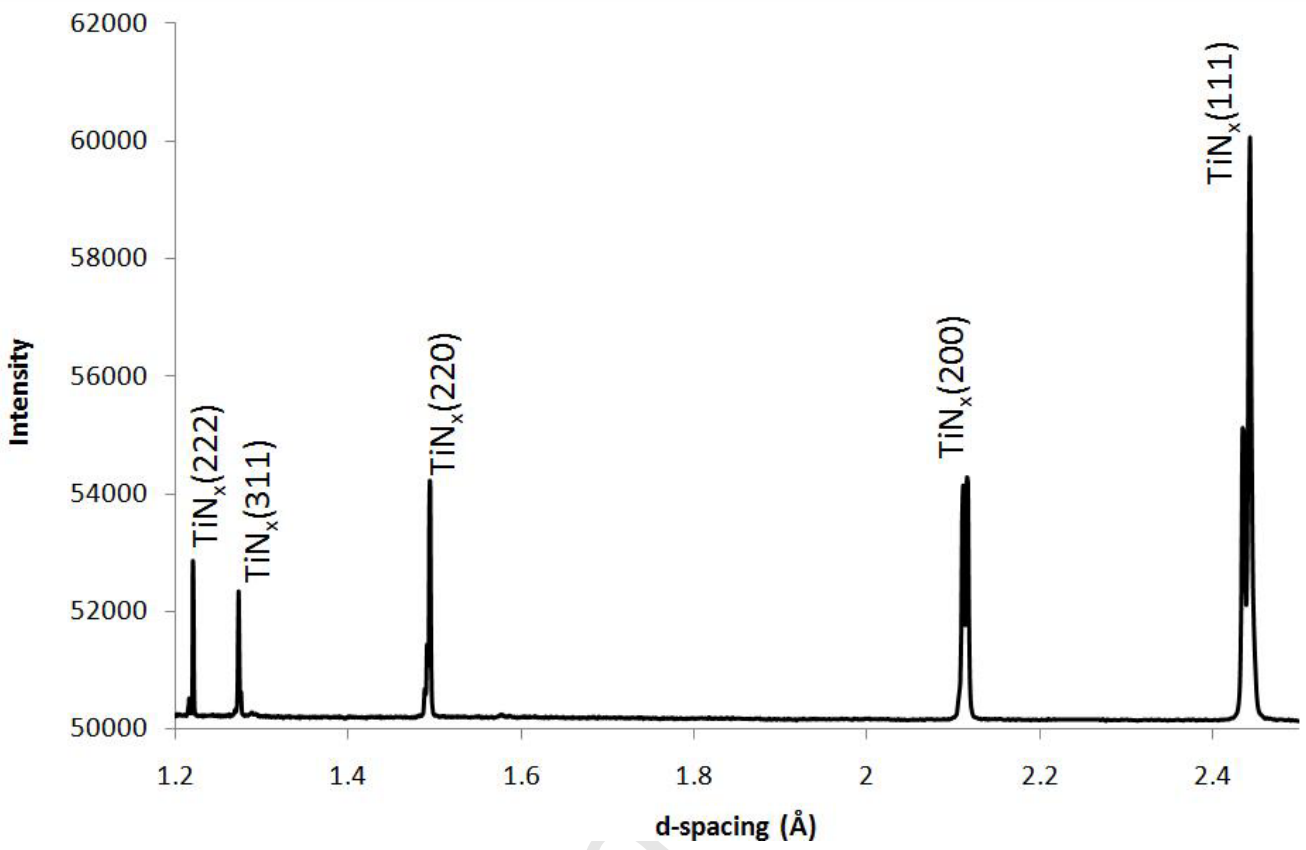

Figure 3: Synchrotron radiation diffraction pattern showing the formation of TiN_x at the near-surface of vacuum-decomposed Ti_2AlN at 1550 °C.

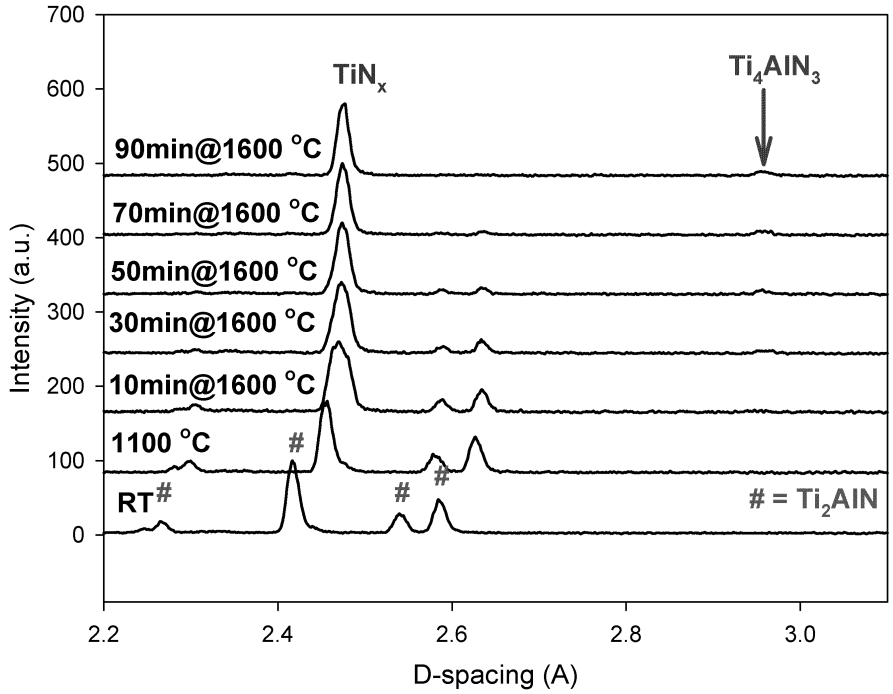

(a)

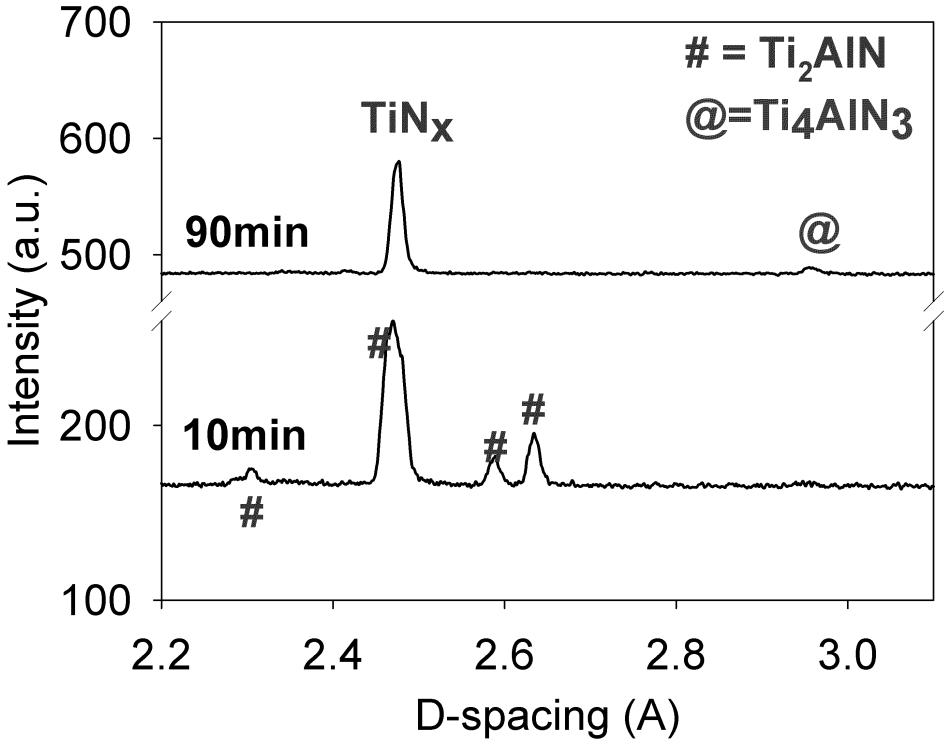

(b)

Figure 4: (a) Diffraction patterns of Ti_2AlN at room temperature (RT), 1100 and 1600°C with dwell times of 10, 30, 50, 70, and 90 minutes. Note that the formation of Ti_4AlN_3 at 1600°C; (b) A close-up view of the time-dependent growth of Ti_4AlN_3 phase at 1600 ºC.

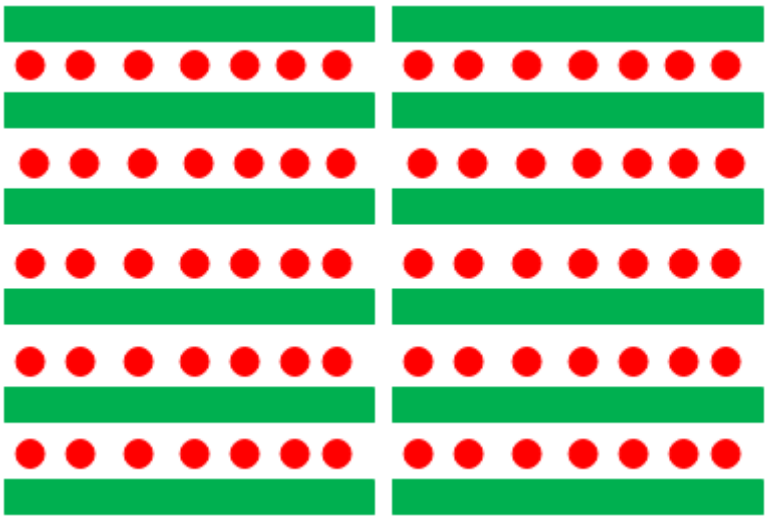

(a)

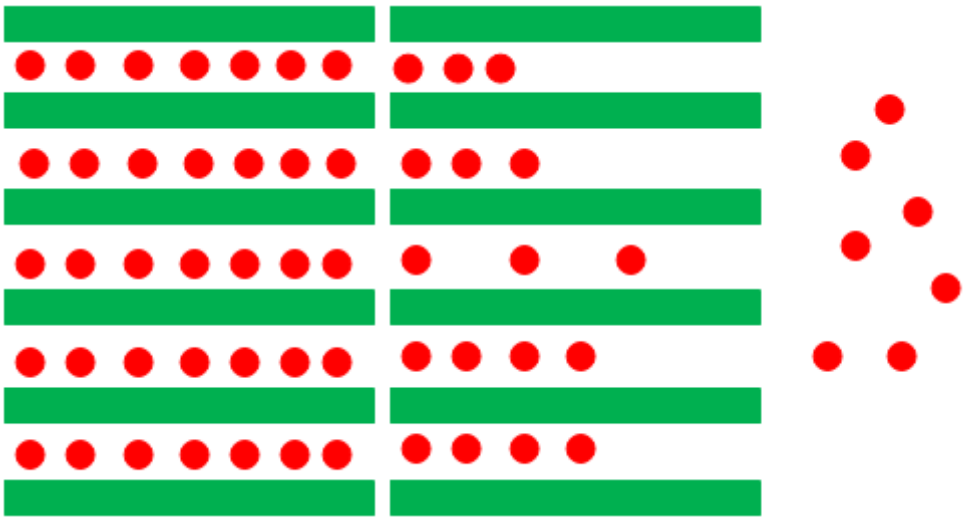

(b)

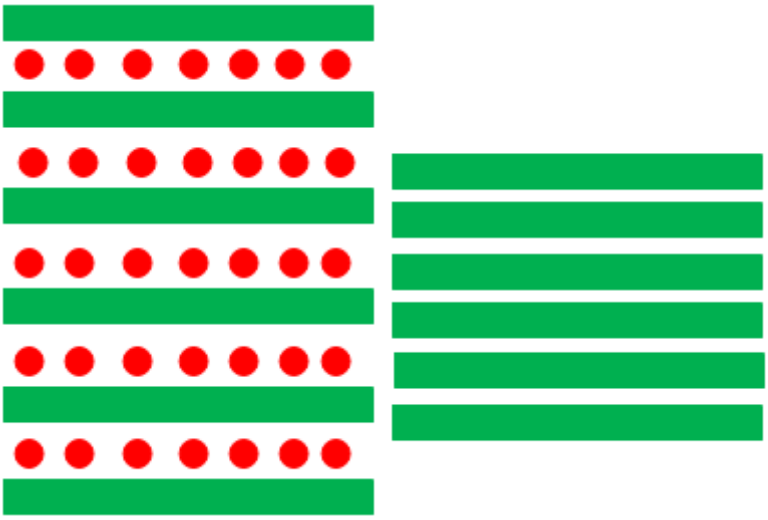

(c)

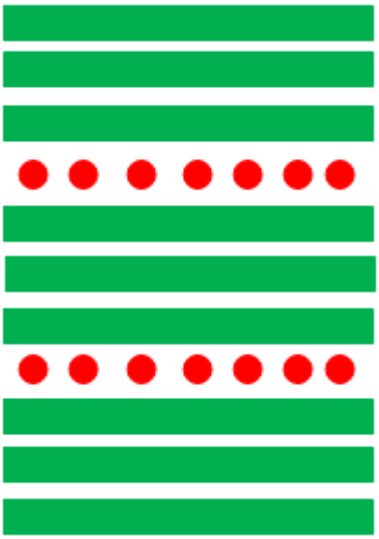

(d)

Figure 5: Schematics showing the formation of Ti_4AlN_3 during the decomposition of Ti_2AlN *via* intercalation with TiN: (a) Ti_2AlN layered structure, (b) exclusion of Al *via* sublimation in vacuum, (c) formation of TiN from total depletion of Al in Ti_2AlN, and (d) intercalation of TiN into Ti_2AlN structure to form Ti_4AlN_3. (Legend: green bar = edge-sharing octahedral NTi_6, red circle = Al element)

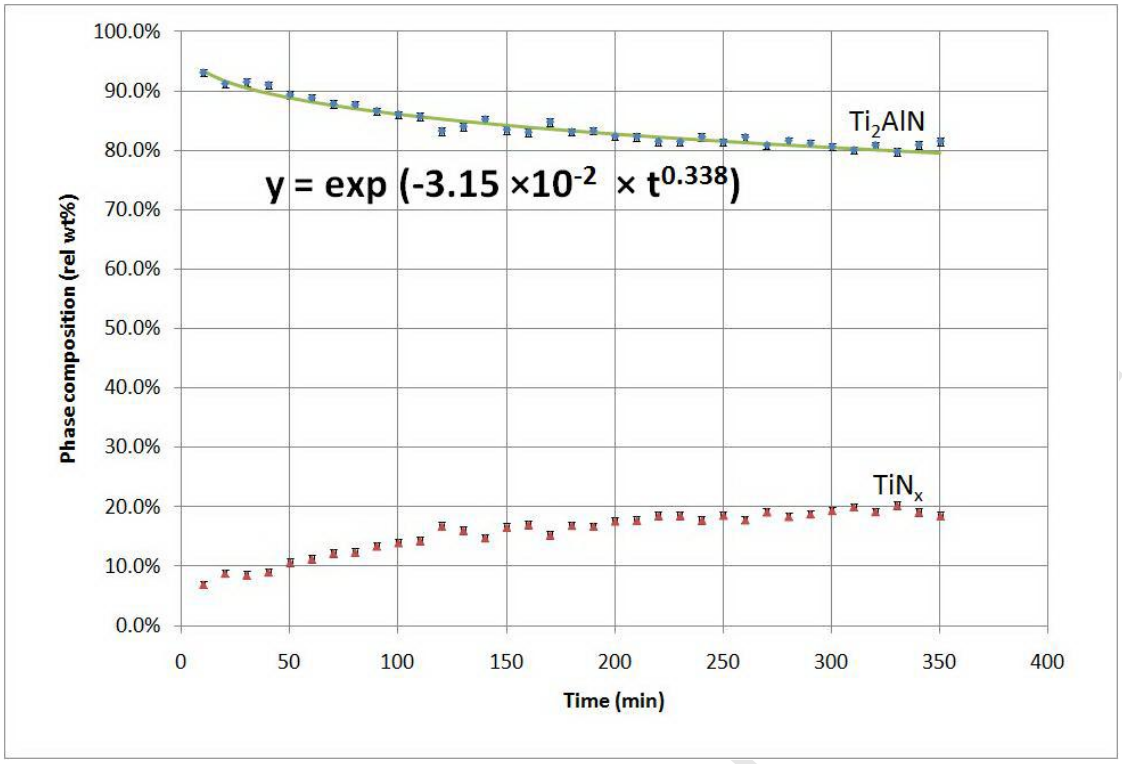

(a)

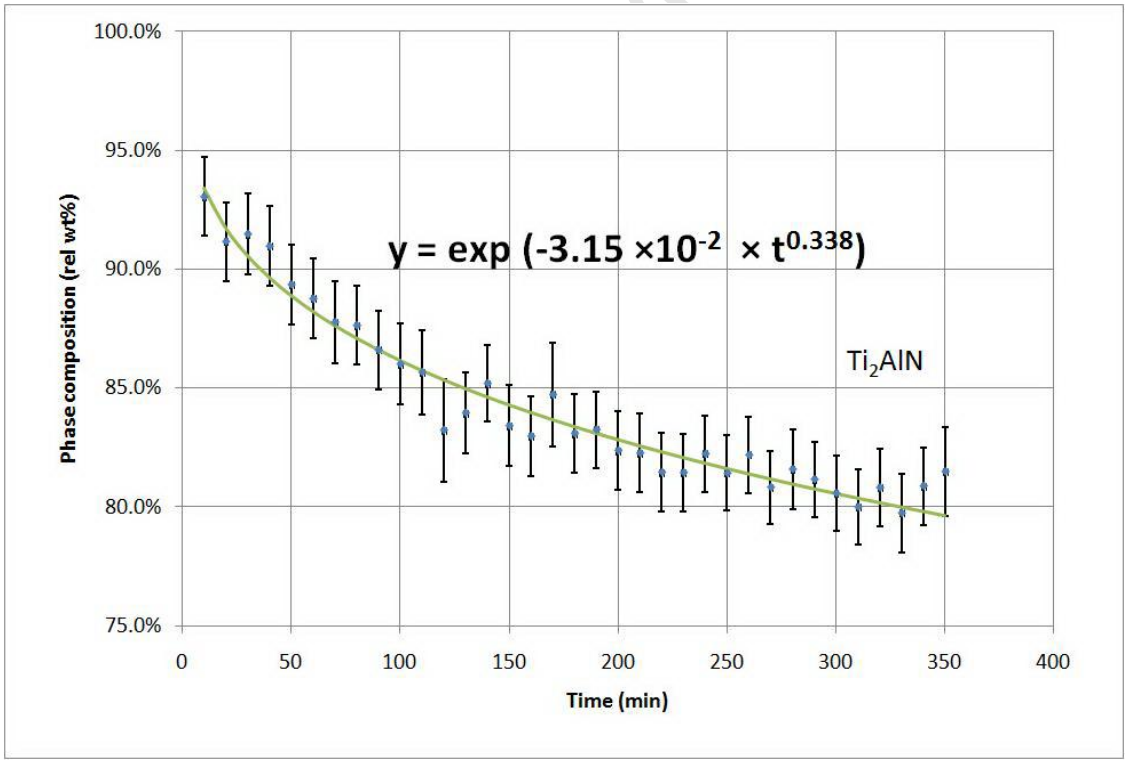

(b)

Figure 6: (a) Phase evolution of Ti_2AlN at 1550 °C as a function of time and (b) reduction of Ti_2AlN showing the fitting with Avrami equation.

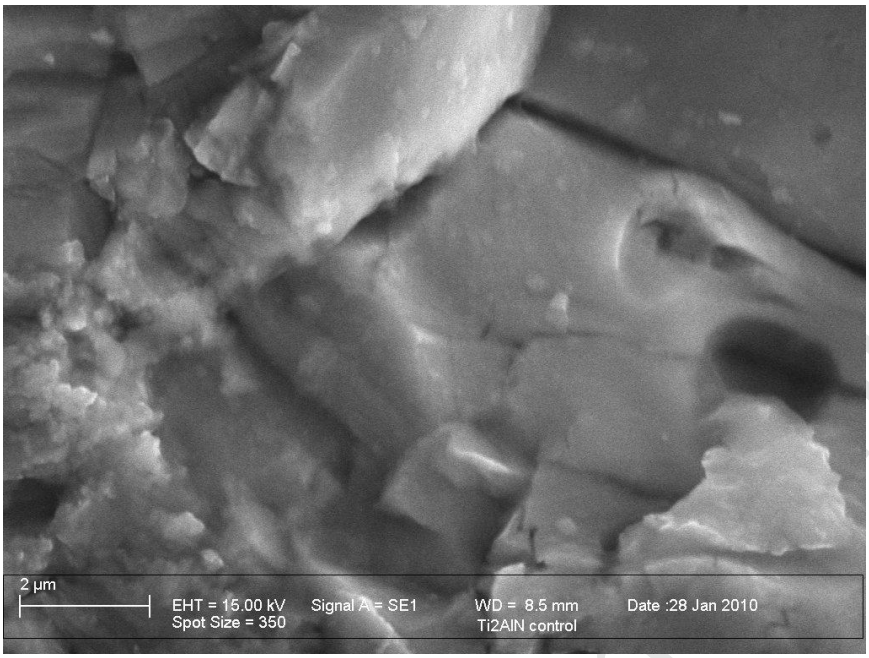

(a)

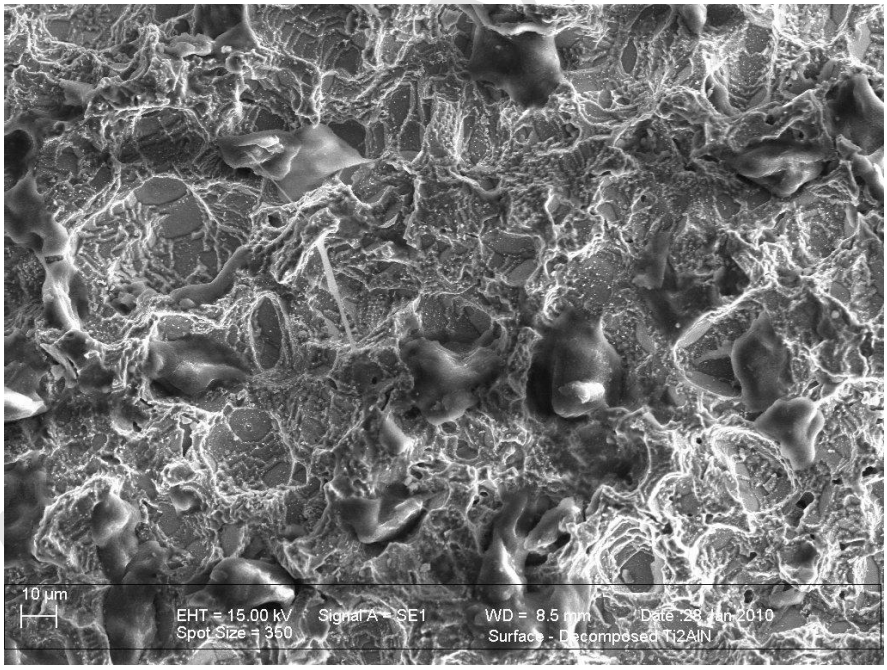

(b)

Figure 7: SEM micrographs showing the surface microstructure of Ti_2AlN; (a) as-received and (b) after vacuum-annealing at 1550 °C.

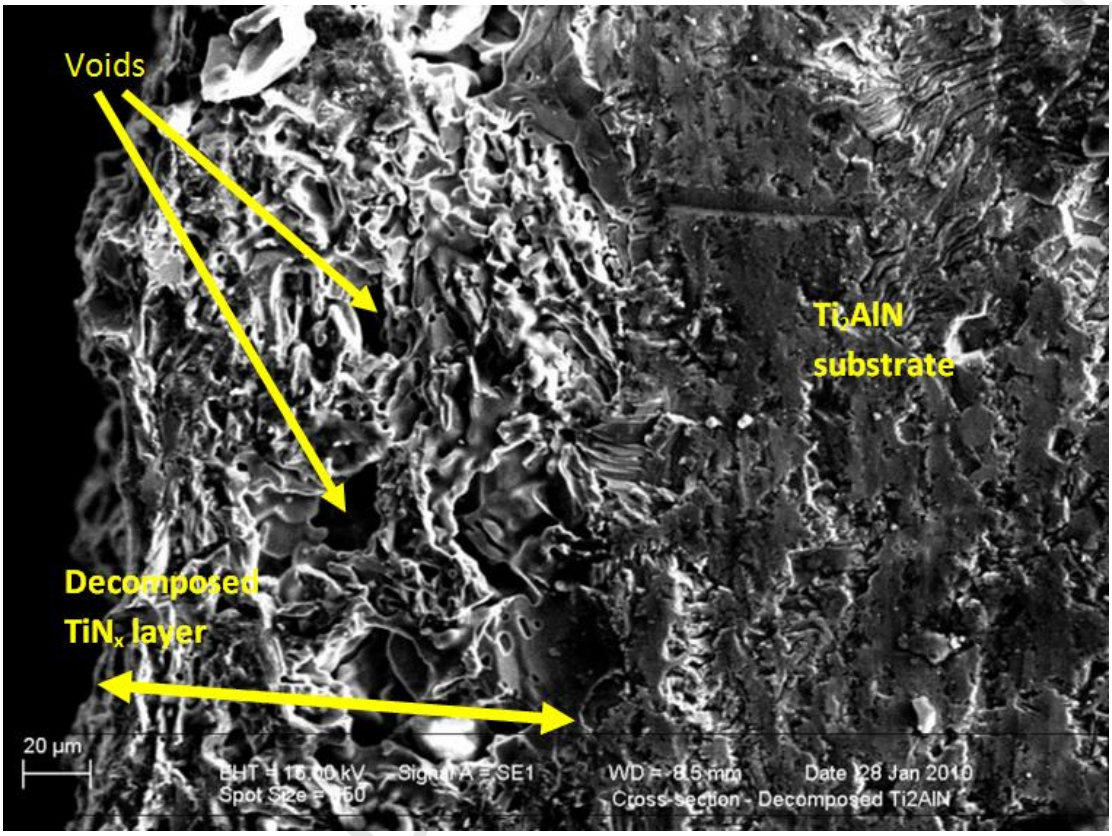

Figure 8: SEM micrograph showing the cross-sectional surface features of vacuum-decomposed Ti_2AlN at 1550 °C.